International Journal of Remote Sensing
Vol. 29, Nos. 17–18, September 2008, 5093–5111

Model inversion for chlorophyll estimation in open canopies from hyperspectral imagery

P. KEMPENEERS*†, P. J. ZARCO-TEJADA‡, P. R. J. NORTH§, S. DE BACKER¶, S. DELALIEUX**, G. SEPULCRE-CANTÓ‡, F. MORALES††, J. A. N. VAN AARDT‡‡, R. SAGARDOY††, P. COPPIN** and P. SCHEUNDERS¶

†Flemish Institute for Technological Research (VITO), Boeretang 200 B-2400 Mol, Belgium
‡Instituto de Agricultura Sostenible (IAS-CSIC), Córdoba, Spain
§University of Wales Swansea, Swansea SA2 8PP, United Kingdom
¶Universiteit Antwerpen, Universiteitsplein 1, B-2610 Antwerpen, Belgium
**Katholieke Universiteit Leuven, Celestijnenlijn 200E, B-3001 Heverlee, Belgium
††Estación Experimental Aula Dei (EEAD-CSIC), Zaragoza, Spain
‡‡CSIR - NRE Ecosystems Earth Observations, P.O. Box 395, Pretoria 0001, South Africa

(*Received 4 December 2006; in final form 6 April 2007*)

This paper presents the results of estimation of leaf chlorophyll concentration through model inversion, from hyperspectral imagery of artificially treated orchard crops. The objectives were to examine model inversion robustness under changing viewing conditions, and the potential of multi-angle hyperspectral data to improve accuracy of chlorophyll estimation. The results were compared with leaf chlorophyll measurements from laboratory analysis and field spectroscopy. Two state-of-the-art canopy models were compared. The first is a turbid medium canopy reflectance model (MCRM) and the second is a 3D model (FLIGHT). Both were linked to the PROSPECT leaf model. A linear regression using a single band was also performed as a reference. The different techniques were able to detect nutrient deficiencies that caused stress from the hyperspectral data obtained from the airborne AHS sensor. However, quantitative chlorophyll retrieval was found largely dependent on viewing conditions for regression and the turbid medium model inversion. In contrast, the 3D model was successful for all observations. It offers a robust technique to extract chlorophyll quantitatively from airborne hyperspectral data. When multi-angular data were combined, the results for both the turbid medium and 3D model increased. Final RMSE values of $5.8\,\mu g\,cm^{-2}$ (MCRM) and $4.7\,\mu g\,cm^{-2}$ (FLIGHT) were obtained for chlorophyll retrieval on canopy level.

1. Introduction

Hyperspectral remote sensing has the potential to estimate leaf biochemical constituents such as chlorophyll concentration (C_{ab}) from airborne image acquisition. By quantifying photosynthetic pigments in agricultural crops their physiological state can be assessed. Several studies have introduced narrow-band

*Corresponding author. Email: pieter.kempeneers@vito.be

International Journal of Remote Sensing
ISSN 0143-1161 print/ISSN 1366-5901 online © 2008 Taylor & Francis
http://www.tandf.co.uk/journals
DOI: 10.1080/01431160802036458

spectral indices to this end (Carter 1994, Peñuelas *et al.* 1994, 1995a,b, Gamon 1992). More specifically, (Daughtry *et al.* 2000, Zarco-Tejada *et al.* 2001, Lichtenthaler *et al.* 1996, Gitelson and Merzlyak 1996, Haboudane *et al.* 2002) derived indices for chlorophyll content estimation allow us to detect chlorosis in an early stage. Independent estimation of chlorophyll has also been shown to have the potential to improve ecological models of net primary productivity (NPP) driven by satellite data (Dawson *et al.* 2003).

One of the difficulties with these indices is that they are responsive to other vegetation and environmental parameters such as LAI, and underlying soil reflectance (Daughtry *et al.* 2000, Kim *et al.* 1994, Zarco-Tejada *et al.* 2004). Relationships obtained at leaf level cannot be transferred to the canopy level. Derivative indices are proposed, especially related to the red edge (Miller *et al.* 1990), to estimate chlorophyll at both leaf and canopy levels. However, structure and canopy architecture is critical and can cause the empirical relationships to fail on other canopies. Moreover, the relationships at canopy level must be tuned for spectral and spatial sensor characteristics and viewing conditions (Myneni *et al.* 1995, Verstraete *et al.* 1996). Due to the sensitivity of indices to these extraneous factors, the accurate estimation of biochemical constituents on a routine basis remains problematic.

Jacquemoud *et al.* (2000), Kuusk (1998) and Weiss *et al.* (2000) inverted coupled leaf-canopy radiative transfer models to estimate leaf biochemistry. The canopy model should compensate for canopy structure and viewing geometry. However, for open crop canopies, where soil background and shadows dominate the bidirectional reflectance signature, this is far from evident. Zarco-Tejada *et al.* (2004) found PROSPECT-SAILH results derived for pure crowns to be inaccurate when applied to pixels with aggregated soil background and shadow scene components. On the other hand, more realistic and more accurate models become available, along with cheaper computing power to run them.

The objective of this paper is to demonstrate (and quantify) the dependence of the accuracy of chlorophyll retrieval on viewing conditions on canopy level in a peach orchard. This is important if remote sensing is to be applied as an operational tool for precision agriculture. For satellite sensors with large swaths, the prerequisite of nadir viewing is seldom met. But high spatial resolution sensors suffer from suboptimal viewing conditions as well. They must be pointed to off-nadir positions to obtain an acceptable revisit time.

We compared two canopy models in our study. They were linked to the PROSPECT leaf model (Jacquemoud *et al.* 1996). The first, MCRM (Kuusk 1995), assumes the canopy layer as a turbid medium. It does not take into account tree crown closure, tree density, height, shape and dimension of crowns. The second is the 3D geometric-optical model, FLIGHT (North 1996). It is a more realistic model based on ray tracing, accounting for influences of canopy architecture on reflectance. Bidirectional reflectance effects are calculated as a function of the illumination and viewing geometry and scene components such as shadow and soil effects. This is an advantage over the first type of models with respect to the robustness of viewing geometry, as will be shown.

We then investigated how multi-angular remote sensing data can increase the accuracy of the chlorophyll estimation. Multi-angular viewing data are now available. For example, the MISR (Multi-angle Imaging SpectroRadiometer, Diner. *et al.* 1998) instrument onboard NASA's Terra satellite has nine sensors with

different viewing angles and the CHRIS (Compact High Resolution Imaging Spectrometer, Barnsley *et al.* 2004) instrument is pointable off-nadir in both the along-track and across-track direction, by tilting the PROBA platform. For this study, the peach orchard was imaged in four tracks with the AHS airborne hyperspectral sensor with different viewing geometries. We tested different techniques to combine the multi-angular that improved the accuracy of chlorophyll retrieval. Still, the 3D model outperformed the turbid medium mode (5.8 $\mu g\,cm^{-2}$ for MCRM and 4.7 $\mu g\,cm^{-2}$ for FLIGHT).

2. Methodology

Biochemical parameters of crops can be estimated more accurately, with the introduction of hyperspectral sensors. The large number of narrow bands allow us to measure absorption features more precisely. For chlorophyll, absorptions are located in the visible region of the spectrum (Curran 1989). Several methodologies exist to estimate the concentration of chlorophyll from remote sensing data.

2.1 *Data analysis*

The chlorophyll value measured *in situ* can be used as the response value in a regression analysis. The explanatory variable is the reflectance value in one (simple linear regression) or more bands (multiple regression). Wessman *et al.* (1988), Curran *et al.* (1992) and Martin and Aber (1997) derived a predictive algorithm for chlorophyll from a training data set, by estimating the statistical relationship between the chlorophyll concentration and the specific bands of leaf or canopy reflectance.

Camps-Valls *et al.* (2006) suggested a robust regression, based on support vector machines that is particularly useful in the case of limited *in situ* measurements. Regression can be performed both on leaf level and on canopy level.

We performed a simple linear regression. No improvements were found using multiple linear regression. The optimal band was selected from an optimization scheme, minimizing the residual sum of squared errors between the estimated and measured chlorophyll concentrations in the training set (feature selection).

Grossman *et al.* (1996) demonstrated that the predictive algorithm obtained from regression, trained on a specific site and crop, is not reliable for other conditions. The selected bands depend on the data set at hand, influenced by species, canopy structure and viewing conditions. Several techniques have been introduced to increase the robustness of biochemical parameter estimation, including continuum-removal (Kokaly and Clark 1999), band ratios (Chappelle *et al.* 1992, Blackmer *et al.* 1996) and normalized differences (Kim *et al.* 1994, Daughtry *et al.* 2000).

2.2 *Model inversion*

Another technique to retrieve chlorophyll from reflectance data is through inversion of leaf and canopy reflectance models. Inversion is usually performed numerically with an iterative optimization method. The forward model can be applied directly at each iteration, though lookup tables might be a better option if performance is critical (Knyazikhin *et al.* 1998, Pragnère *et al.* 1999). Neural networks have also been shown to be efficient to invert canopy models (Smith 1993, Abuelgasim *et al.* 1998, Kimes *et al.* 1998, Schlerf and Atzberger 2006).

Foliar chlorophyll can be retrieved from leaf reflectance by inverting a leaf radiative transfer model. We selected PROSPECT version 2.01 (10 April 1995), with five input parameters: Chlorophyll a + b (C_{ab} in $\mu g\,cm^{-2}$), leaf structure (N), leaf water equivalent thickness (Cw in cm), leaf protein content (Cp in $g\,cm^{-2}$), and leaf cellulose + lignin content (Cc in $g\,cm^{-2}$).

To estimate biochemical parameters from canopy reflectance, the leaf model must be coupled with a canopy model. For this goal, we used two different canopy models.

MCRM (Kuusk 1995), a Markov chain model of canopy reflectance, calculates the radiative transfer within vegetation canopies. It is based on the homogeneous multispectral model MSRM (Kuusk 1994) and the SAIL (Verhoef 1984) model, which models the diffuse radiative transfer. The MCRM model accounts for non-Lambertian soil reflectance, specular reflection of direct Sun rays on leaves, the hot spot effect, a two-parameter leaf angle distribution (LAD) and the spectral effect of cultivation rows.

The second is the 3D geometric-optical model, FLIGHT (North 1996). It has been developed to efficiently simulate the spectral reflectance for a specific Sun-sensor geometry, and to estimate canopy photosynthesis (Barton and North 2001, North 2002, Alton *et al.* 2005). A recent intercomparison with a set of six Monte Carlo models shows agreement with ≈1% dispersion in reflectance (Pinty *et al.* 2004).

The numerical inversion minimizes a merit or cost function. This is typically the sum of squared differences between the measured and modelled canopy spectral reflectance in each spectral band ($i=1, \ldots, d$) (1):

$$\Delta^2 = \frac{1}{d}\sum_{i=1}^{d}\left(R_i - \hat{R}_i(P)\right)^2. \quad (1)$$

The modelled reflectance $\hat{R}$ depends on the model parameters P. The optimization thus consists of finding the optimal model parameters P that minimize the merit function. Although some typical canopy parameters such as leaf area index (LAI) and Sun and viewing angles remain the same, others are model specific. The number of parameters is also different for the two models. A well known problem of model inversion is that it is ill posed. Different parameters interfere and multiple parameter sets may lead to the same solution. It is therefore important to constrain most of the parameters or fix them to their known (measured) values. Reducing the number of parameters to be optimized is also required for performance reasons.

Modifications of the merit function (1) exist, for example by weighting the contributions of the individual wavelengths. Zarco-Tejada *et al.* (2001) used merit function based on an optical index R_{750}/R_{710} focusing on a single band ratio, rather than the entire spectrum. The authors showed superior results, especially if reflectance signals included shadowed pixels. We used the unweighted merit function (1), but we focused on the green peak for inverting FLIGHT ($d=7$, from 455 nm to 601 nm). Moreover, the signal-to-noise ratio in the SWIR region of the AHS sensor proved to be very low.

If multi-angular data are available, the extra information can be used to increase the accuracy of the parameter estimation. This can be done in different ways. For n observations, we can extend the definition of the merit function

(Weiss *et al.* 2000):

$$\sum_{j=1}^{n} \Delta_j^2 = \frac{1}{n}\frac{1}{d}\sum_{j=1}^{n}\sum_{i=1}^{d}\left(R_{i,j} - \hat{R}_{i,j}(P_j)\right)^2, \tag{2}$$

where subscript j indicates the observation. We will refer to this as the *direct mode*, because multi-angular data are used directly within the optimization process. In contrast, we can use the obtained results for each observation in a *posterior* mode, by just averaging the individual results. The direct mode will better constraint the optimization process and is probably preferred if more parameters must be estimated simultaneously. Likewise, if the model is not robust to different observation conditions, the individual results are not reliable and must not be combined. However, in case of a robust model, averaging the individual results might be a good alternative, as will be shown in § 4.

The modelled reflectance $\hat{R}$ was filtered to obtain a simulated reflectance signature that is consistent with the reflectance measured by the airborne hyperspectral sensor. Specifically for the AHS sensor with a varying bandwidth, it is important to match the modelled spectrum to the sensor specifications. Figure 1 shows the modelled spectrum before and after filtering.

Biochemical leaf parameters (other than chlorophyll) were not measured so all five PROSPECT parameters were estimated simultaneously. For the optimization we selected ASA, an adapted simulating annealing (Ingber undated), which is robust to local minima. We chose only to optimize for chlorophyll for the MCRM model, fixing all remaining parameters. For the FLIGHT model, we estimated fraction cover in addition to chlorophyll, motivated by the uncertainty on the tree extraction in the image, due to the coarse resolution with respect to the crown size. The fraction cover was estimated between 0.6 and 0.9, relating to the understorey between the tree rows in the orchard. Understorey spectra were extracted from the image data and averaged as input for the model.

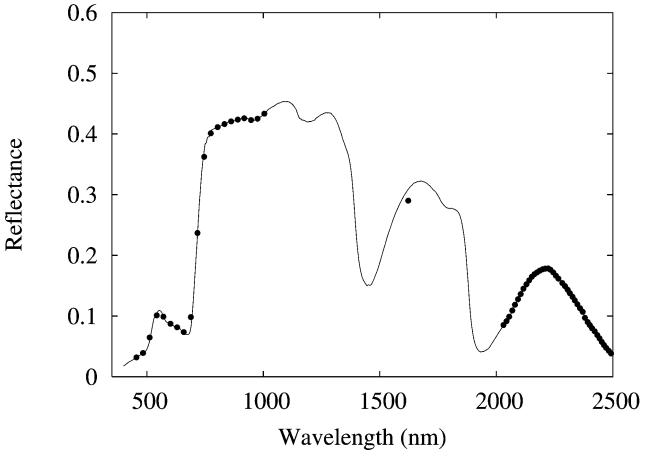

Figure 1. The modelled canopy spectrum before (solid) and after (dots) filtering according to the specifications of the AHS sensor.

3. Experiments

3.1 *Experimental setup*

A peach orchard near Zaragoza, Spain (Lat: 41°28′ N, Long: 1°22′ W) was chosen as a test case to experiment with the chlorophyll retrieval techniques. It was treated with iron chelates to recover from iron chlorosis conditions. The orchard, represented as a matrix, consists of 35 rows and six columns. The total number of trees is only 205 instead of 210, because five trees are missing. Iron chlorosis is induced in 48 trees, located in the two rightmost columns of the orchard, schematically presented in figure 2. Trees are represented, and treated, in blocks of three. As an exception, the blocks at the upper end of the plot only contain two trees. The treatment consisted of an iron chelate with four different concentrations (figure 2): 0 g tree^{-1}, 60 g tree^{-1}, 90 g tree^{-1} and 120 g tree^{-1}.

The objective was to create a dynamic range of chlorophyll concentration. Column 3 contained 12 trees (four blocks of three) that were grafted during the previous year (2004).

3.2 *Field data collection*

Fresh leaves are sampled for each tree and measured with the ASD spectrometer using a Leaf Clip. Leaf reflectance was obtained for 716 leaves. We used a SPAD-502 Minolta Chlorophyll Meter for measuring foliar chlorophyll. The SPAD values were calibrated by comparing the SPAD values to chlorophyll concentrations derived from destructive chemical analysis in the laboratory for a subset of leaf

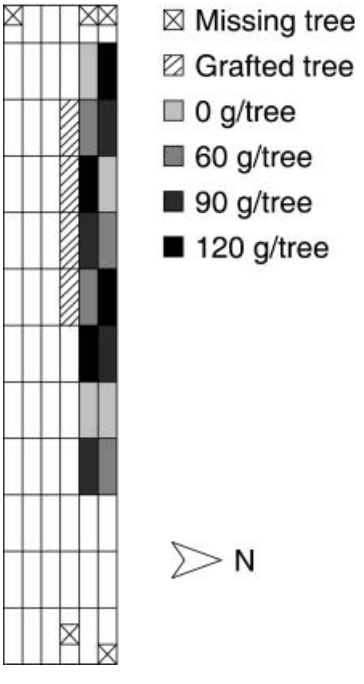

Figure 2. Schematic overview of the orchard. Trees are grouped per 3 (except for upper row). In total, 48 trees in the two rightmost columns were treated with iron chelate with four different concentrations (from light to dark). Column 3 contains 12 trees that were grafted during the previous year.

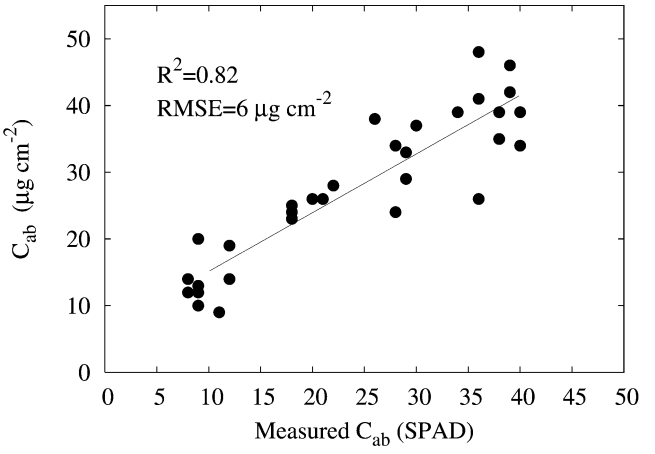

Figure 3. Calibration of the SPAD values using C_{ab} concentrations derived from chemical analysis in the laboratory.

samples. The result is shown in figure 3. A correlation coefficient of 0.82 was obtained with a RMSE of 6.0 $\mu g\,cm^{-2}$. The values are then averaged per tree to compare with parameters obtained on canopy level. The plot average for chlorophyll content is 36.9 $\mu g\,cm^{-2}$, with a variance of 53.4 ($\sigma=7.3$). Extreme values range from 13.7 to 45.7 $\mu g\,cm^{-2}$, showing a large dynamic range as intended.

In addition to chlorophyll, leaf area index was estimated with an LAI2000 instrument for 10 trees. The calculations for LAI were performed according to Villalobos *et al.* (1995), resulting in a mean value of 2.

3.3 *Airborne hyperspectral data*

The AHS sensor has 63 bands covering the visual and near infrared part of the spectrum (450–2500 nm). It was mounted on a CASA C-212 airplane and operated by INTA. The peach orchard was acquired on 12 July 2005 in cloud free conditions (figure 4). Four tracks were flown with different headings (figure 5). The tracks were headed with a 45° difference, with track 1 perpendicular to track 3 and track 2 perpendicular to track 4. The individual tracks fully covered the peach orchard, so that each pixel was acquired with four different view angles. Optimal flight conditions are for track 1, corresponding to a flight path in (and measurements perpendicular to) the solar plane (heading away from the Sun). The small peach orchard is located in the centre of each track, leading to near nadir observations. The pixels were thus selected from a narrow range in the image, where relative azimuth angles correspond to a continuous transition from the left/right part of each scene with respect to nadir. As an example, selected pixels for track 1 were not observed with the expected relative azimuth angles of 90° and 270°. This is illustrated by the scatterplot in figure 6, which schematically shows the view zenith and relative azimuth angles for each pixel and for the different tracks. View zenith is minimum for track 1 (between 4° and 5°), and maximum for track 3 (near to 10°). Tracks 1 and 4 are acquired in backward scatter, and tracks 2 and 3 in forward scatter.

Image data were processed to top of canopy level, using in-house developed software (Biesemans and Everaerts 2006). Atmospheric correction is based on MODTRAN. The integrated atmospheric correction is equivalent to the ATCOR4 theory (Richter 2004). Corrections are made column dependent in order to account

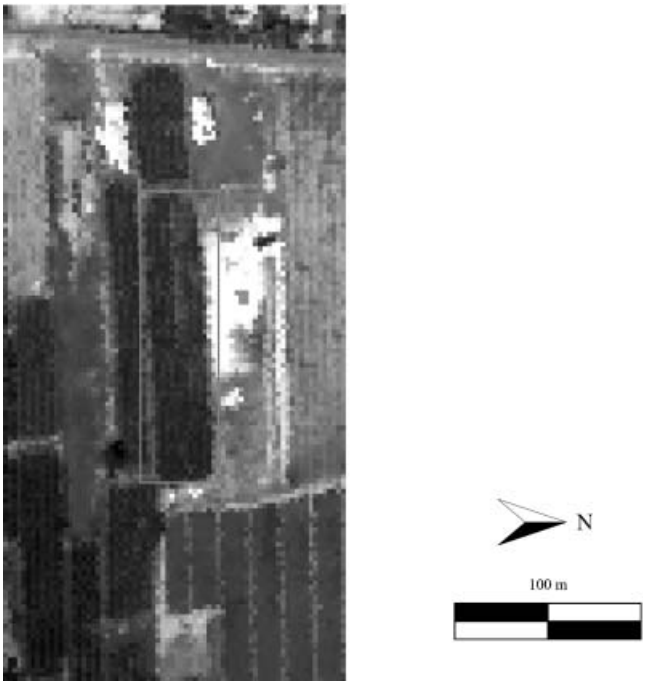

Figure 4. Grey scale image of the orchard acquired with the AHS airborne hyperspectral sensor. The white (WT) and dark (DT) reference targets are visible on the right hand site of the orchard.

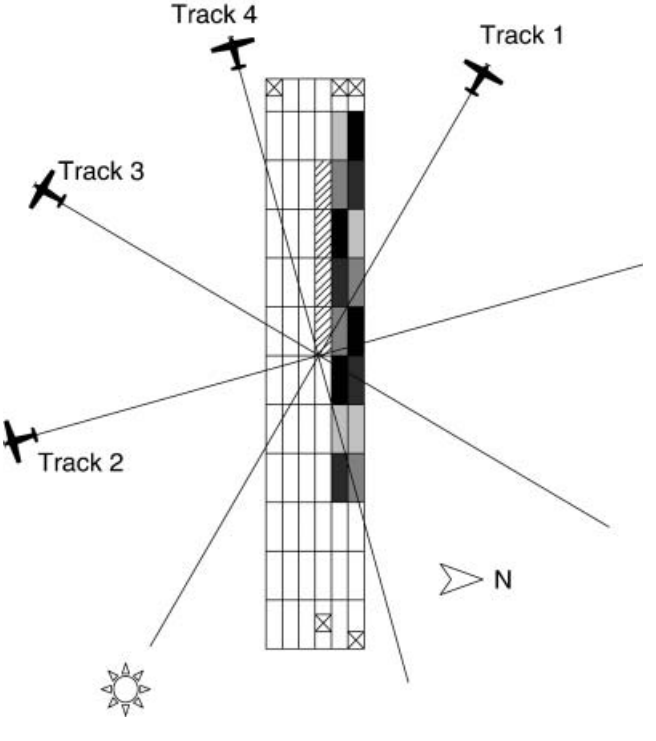

Figure 5. Schematic view of the peach orchard with headings for the four tracks.

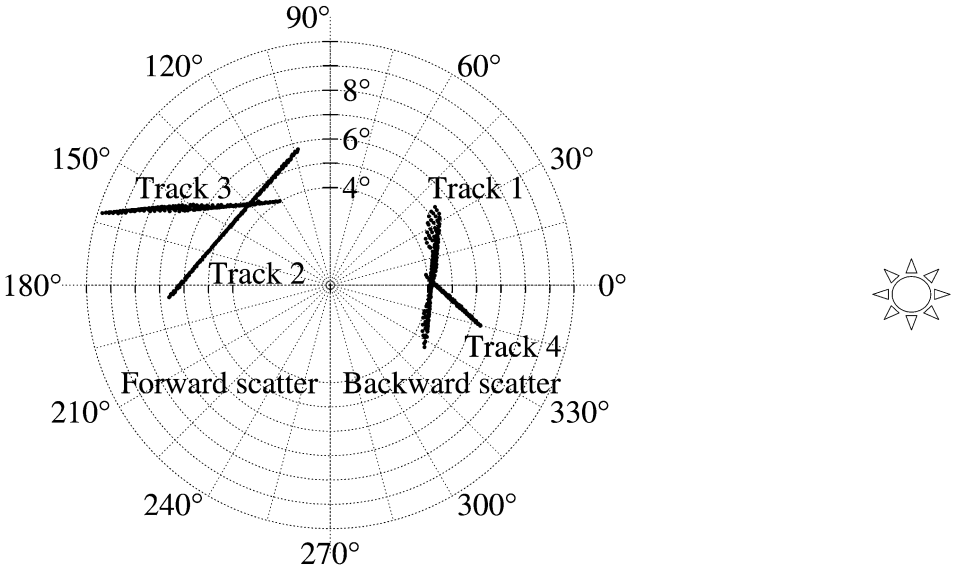

Figure 6. Polar plot of relative azimuth and zenith viewing angle for each track. The individual tracks fully covered the peach orchard, resulting in four different observations for each pixel (represented as dots).

for the different atmospheric paths across AHS images properly. If one single set of atmospheric parameters were used instead, meaning that all the columns in the image are processed assuming one single observation angle, angular variations detected in the chlorophyll estimations could be due to atmospheric effects. We improved the traditional ATCOR approach: instead of using a single LUT (LookUp Table), we created a customized LUT for each image, which is adapted to the specific spectral bands of the sensor and the relevant geometry space obtained during geometric correction. The customized LUT was calculated using a single platform elevation (983 m) and solar zenith angle (27.75°), three view zenith angles and five relative azimuth angles. The atmospheric correction used *in situ* measured parameters, e.g., sunphotometer measurements and ASD spectral measurements over white and dark reference targets. The pixel positions were calculated using GPS measurements and orientation parameters (by means the Inertial Measurement Unit) onboard the airplane. The image was geocoded in a Universal Transverse Mercator projection system (UTM, Zone 30 North, datum WGS84). A subpixel accuracy was obtained after geometric correction with a digital elevation model of the site. The ground resolution of 2.5 m was similar to the crown diameter, which complicated tree identification in the image. The peach trees have been planted according to the scheme in figure 2 every 4 metres ($\frac{8}{5}$ pixels). To facilitate the tree extraction, the hyperspectral image is upsampled with a factor of 5 (with nearest neighbour). Hence, a tree is covered in a region of interest (ROI) with an integer number of (sub)pixels. Using nearest neighbours, the subpixels contain exactly the same spectral information as the original pixels. To obtain the target canopy reflectance, we then took the median reflectance of the subpixels in the ROI. An alternative is to select the pixel in the ROI with maximum NDVI (Normalized Difference Vegetation Index, Rouse *et al.* 1973) or maximum NIR value to minimize the influence of shadows and understorey (canopy openings between rows) as in

Zarco-Tejada *et al.* (2001). However, in our case a ROI can contain subpixels of neighbouring trees due to a combination of: imperfect tree positioning, linked up ROIs and upsampling. To reduce the effect of geometrical inaccuracy and the limited spatial resolution, we averaged the estimated values for a block of three neighbouring trees. This choice was also motivated by the way in which the trees were treated (§ 3.1). On canopy level, we estimated chlorophyll for these individual blocks. This has a severe impact on the variance of the chlorophyll estimation results. This should be taken into account when results are compared to similar studies in the literature. In most cases, larger areas of plots are aggregated, reducing noise and edge effects. With respect to the potential of the proposed techniques for precision agriculture, we chose to assess the crop status with a considerable detail.

4. Results and discussion

We started from leaf level before scaling up to the canopy level. This step-wise approach allowed us to assess the performance of the selected leaf radiative transfer model without entering the complexity of the canopy level. Second, by inverting the leaf model to extract foliar chlorophyll, other biochemical parameters were estimated as well, which could then be constrained on canopy level. A simple linear regression served as a reference, rather than a final goal. It demonstrates the capability to derive chlorophyll with a good accuracy from leaf/canopy reflectance. Furthermore, it was shown that a single band contained sufficient information for this purpose.

4.1 *In situ data: leaf level*

A predictive algorithm was first derived from a simple regression applied to the ASD leaf spectra. As we were not interested in the results on leaf level as such, we averaged the estimated chlorophyll for all leaves in a single tree. We thus obtained a RMSE value of 1.78 $\mu g\,cm^{-2}$ on a tree level, obtained from the leaf spectra. In a second step, we filtered the ASD spectra with the AHS spectral response function (SRF) to check if the AHS sensor was sufficiently conceived for the task of chlorophyll retrieval. In fact little degradation was observed due to the filtering process as shown in figure 7 (RMSE value increased from 1.78 to 2.03 $\mu g\,cm^{-2}$).

An interesting aspect of the filtering process was that the optimal band for simple linear regression shifted from the red edge (702 nm) toward the green peak (571 nm). As expected, for narrow bands, the red edge provides valuable information on chlorophyll. However, for broader bands, the green peak was better suited for this experiment.

We obtained good results with the inversion of PROSPECT, although the RMSE was not as low as with regression (6.48 $\mu g\,cm^{-2}$ and $R^2=0.78$, figure 8).

All five PROSPECT parameters were estimated simultaneously by the optimization routine. Table 1 shows the mean values for all leaves measured. Apart from chlorophyll, there was very little variation in biochemical parameters, so we fixed them for further analysis on canopy level.

The next step was to estimate the chlorophyll on a tree level, obtained from the airborne hyperspectral data.

4.2 *Airborne hyperspectral data: canopy level*

The canopy spectra for all 205 peach trees in the orchard were derived from the AHS image as explained in § 3.3. A single spectrum is obtained for each tree, by taking the median reflectance for the corresponding region of interest.

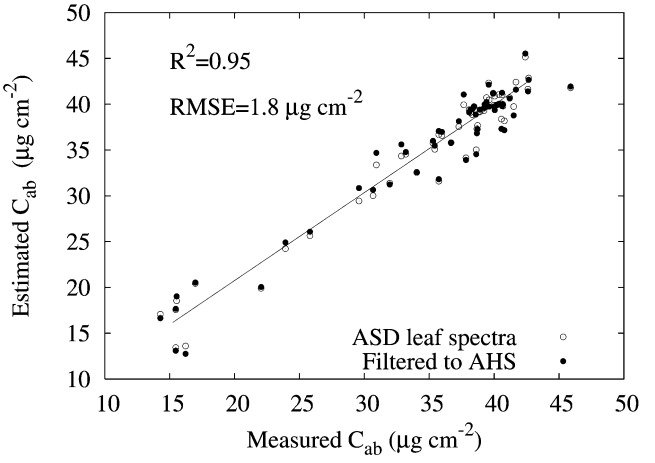

Figure 7. Chlorophyll estimation through simple linear regression of the ASD leaf spectra (solid dots are filtered with the AHS spectral response function).

Similar to the chlorophyll retrieval from leaf reflectance, we performed a simple linear regression. Independent from the leaf level, the same band was selected on canopy level by the feature selection routine in § 2.1, confirming the importance of this spectral region (571 nm). Other than just a reference result on canopy level, the motivation for this was to perform a sensitivity analysis on the viewing conditions. It is a generally known problem that the predictive algorithm is site and crop specific and is not reliable for other conditions (Grossman *et al.* 1996). In this experiment, crop and site (canopy architecture) was fixed. The time difference between the first and last track was 40 minutes with clear sky conditions and thus, atmospheric conditions and illumination geometry were nearly identical for the four tracks as well (difference in atmospheric path length is negligible because of small viewing zenith angles). By training the predictive algorithm on one track and testing on the other, we were able to assess the effect of viewing conditions on the regression

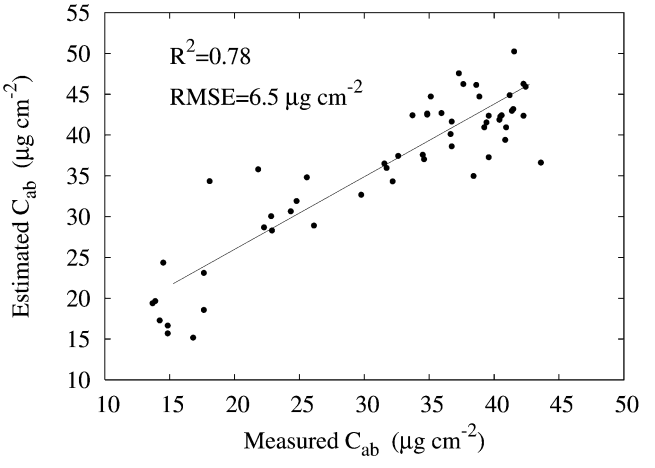

Figure 8. Chlorophyll estimation through inversion of the PROSPECT leaf radiative transfer model for ASD leaf spectra (filtered with the AHS spectral response function).

Table 1. Estimated PROSPECT parameters (mean over all leaves).

Parameter	Value	Variance
Water equivalent thickness (cm)	0.0121	$9.98\ 10^{-7}$
Leaf protein content ($g\,cm^{-2}$)	0.0002	$1.8\ 10^{-20}$
Leaf cellulose and lignin content content ($g\,cm^{-2}$)	0.0031	$1.02\ 10^{-7}$
Elementary layers inside a leaf	1.8	0.0047
Chlorophyll concentration ($\mu g\,cm^{-2}$)	39	98

technique. The results in table 2 show there is an important dependence, as expressed by the variance in the last column for most tracks. The first column indicates the tracks used for training, while those for test are shown in the next columns. As an example, if track 4 was used for training (last row), the RMSE for estimating chlorophyll using data from track 3 was $9.7\,\mu g\,cm^{-2}$. This is more than double the error obtained when testing on the same track (using a leave-one-out cross-validation, Lachenbruch 1967).

We then inverted the radiative transfer models PROSPECT and MCRM. We derived C_{ab} by first fixing the other four parameters for the PROSPECT leaf model to the mean values from table 1. The canopy model parameters were fixed as well. The Sun and view angles were logged for each pixel during the flight and thus could be set to their actual values. The leaf area index (LAI) was fixed to 2, the mean value of the measured subset (§ 3.2). The remaining parameters were fixed to the centre of the model range. The chlorophyll was loosely constrained ($0–60\,\mu g\,cm^{-2}$). An overview of the fixed values or ranges for the MCRM canopy reflectance model is shown in table 3.

The results in the first row of table 5 show the severe impact of the viewing on the performance of the turbid medium model inversion. Best results are obtained for track 1, with a small value for RMSE ($5.2\,\mu g\,cm^{-2}$) and a high correlation coefficient ($R^2=0.44$). This track corresponds to the optimal flight conditions. In contrast, track 3 with its suboptimal viewing conditions result in a high RMSE value of $12.5\,\mu g\,cm^{-2}$ ($R^2=0.5$). In general, chlorophyll is overestimated with forward scatter acquisitions (tracks 2 and 3). Most surprising is that even for the narrow range of view zenith angles (4–10°) chlorophyll estimations with the turbid medium model are that sensitive to relative azimuth angles. Because no reference data were available for pixels with larger zenith angles, we created synthetic data. Using the same turbid medium model in forward mode would be of little relevance due to circular reasoning. We therefore used the 3D FLIGHT model to create the synthetic data and the turbid medium model for inversion. We simulated view zenith angles

Table 2. Assessment of the effect of viewing conditions on simple linear regression. Training was performed using a single track (column 1). RMSE ($\mu g\,cm^{-2}$) and R^2 values of C_{ab} are calculated on the test tracks in row 1 respectively.

RMSE (R^2)	Track 1	Track 2	Track 3	Track 4	Mean	Variance
Track 1	4.5 (0.56)	5.6 (0.52)	6.5 (0.62)	5.3 (0.50)	5.5 (0.55)	0.7 (0.003)
Track 2	5.3 (0.56)	4.8 (0.52)	4.7 (0.62)	6.9 (0.50)	5.4 (0.55)	1.1 (0.003)
Track 3	7.7 (0.58)	5.1 (0.49)	4.4 (0.59)	9.9 (0.60)	6.8 (0.57)	6.4 (0.002)
Track 4	5.1 (0.58)	8.6 (0.49)	9.7 (0.59)	4.5 (0.60)	7.0 (0.57)	6.7 (0.002)

Table 3. Parameters used for the MCRM canopy reflectance model.

Parameter	Value
Solar zenith angle	25–30°
Solar azimuth angle	121–132°
View zenith angle	4.4–6.6°
Relative viewing azimuth	0–360°
Leaf area index	2
Leaf size	0.02
Mean leaf angle (elliptical LAD)	45
Eccentricity of LAD	0.91
Ångström turbidity factor	0.1
Clumping parameter	0.8
Ratio of refractive indices	1
Price weight 1 (soil)	0.2
Price weight 2 (soil)	0
Price weight 3 (soil)	0
Price weight 4 (soil)	0

from 5° to 10° and from 30° to 35° (the AHS sensor provides data with view zenith angles up to 45°). For backward scatter (tracks 1 and 4), there was little impact of larger view zenith angles on the accuracy of chlorophyll estimates. Values for R^2 decreased from 0.98 to 0.86, but RMSE also decreased from 7.7 to 5.8 $\mu g\,cm^{-2}$. In case of forward scattering though (corresponding to tracks 2 and 3), the estimates were influenced for the worst: RMSE values increased from 13 to 17 $\mu g\,cm^{-2}$, with less correlation between estimated and true chlorophyll content (R^2 decreased from 0.84 to 0.6). Similar to our experimental data, there was an overestimation for the chlorophyll content for the forward scattered simulated data.

Finally, we inverted the 3D FLIGHT model coupled with PROSPECT. For performance reasons, a lookup table was used. A lookup table was created for different values of chlorophyll (10–60 $\mu g\,cm^{-2}$), fraction cover (0.6–0.9) and view

Table 4. Parameters used for the 3D canopy reflectance model FLIGHT.

Parameter	Value
Solar zenith angle	27.75°
Solar azimuth angle	126.25°
View zenith angle	5.35°
Relative viewing azimuth	0–360°
Total LAI	2
Leaf size	0.02
Leaf area distribution	spherical
Mode	reverse
Dimension	3
Fraction ground cover	0.6–0.9
Fraction of green cover	1
Number of photons	100 000
Soil roughness index	0.1
Aerosol optical thickness (555 nm)	0.1
Crown radius (m)	1.2
Crown centre to top distance (m)	1
Min height to first branch (m)	1
Max height to first branch (m)	1.5

Table 5. RMSE ($\mu g\,cm^{-2}$) and R^2 values of C_{ab} through model inversion. The 3D model FLIGHT is more robust to viewing conditions than turbid medium model MCRM. Mean and variance values are calculated over RMSE values for tracks 1–4.

RMSE (R^2)	Track 1	Track 2	Track 3	Track 4	Mean	Variance
MCRM	**5.2** (0.44)	9.9 (0.36)	12.5 (0.5)	6.7 (0.38)	8.6 (0.42)	10.5 (0.005)
FLIGHT	**5.4** (0.46)	6.1 (0.42)	6.4 (0.58)	6.9 (0.39)	6.2 (0.46)	0.4 (0.007)

azimuth angle (0–360° in steps of 15°). The Sun angles and view zenith angle (table 3) were approximated to their mean values and fixed in the model. The relevant values (ranges) of the parameter settings for FLIGHT are listed in table 4. Again, best results are obtained for track 1, with RMSE=5.4 $\mu g\,cm^{-2}$ and R^2=0.46. Most importantly, results are much more robust to viewing conditions as shown in row 2 of table 5. Compared to the turbid medium model, variance for RMSE drops from 10.5 to 0.4, with extreme RMSE values between 5.4 and 6.9 $\mu g\,cm^{-2}$ (5.2 and 12.5 $\mu g\,cm^{-2}$ for MCRM). Correlation variates from 0.39 (track 4) to 0.58 (track 3), and is always higher than results from MCRM inversion.

If multi-angular information is available, this information can be used to increase the accuracy of the parameter retrieval. The merit function was adapted according to (2). The obtained RMSE is 5.8 and 5.0 $\mu g\,cm^{-2}$, with a correlation R^2 of 0.48 and 0.52 for MCRM and FLIGHT respectively. Although the 3D model still outperforms the turbid medium model, the difference is small. It should be noted that for this experiment only chlorophyll was estimated. If the optimization scheme must deal with more parameters, the extra constraint of the multi-angular information is expected to be more beneficial. However, for the more robust 3D model, the individual results from the single observations are more reliable and contribute to the best estimation (RMSE=4.7 $\mu g\,cm^{-2}$ and R^2=0.56). The chlorophyll values, estimated using multi-angular information, are plotted against the measured values in the scatterplot of figure 9. Linear regression, RMSE and R^2 are indicated for both models.

5. Conclusions

The effect of viewing conditions on the retrieval of foliar chlorophyll from canopy reflectance is presented. Three techniques were tested on airborne hyperspectral data, acquired with the AHS sensor. The test plot covered a peach orchard, where trees were treated with iron chelates to recover from iron chlorosis conditions. Blocks of trees treated with iron chelates created a dynamic range of chlorophyll concentration as measured in leaves. Multi-angular hyperspectral data were

Table 6. RMSE ($\mu g\,cm^{-2}$) and R^2 values of C_{ab} through model inversion. Multi-angular information is either directly integrated in the model inversion using equation (2) (direct mode) or post-processed by averaging the individual results for each observation (posterior mode).

RMSE (R^2)	Direct mode	Posterior mode
MCRM	5.8 (0.48)	6.1 (0.52)
FLIGHT	5.0 (0.52)	4.7 (0.56)

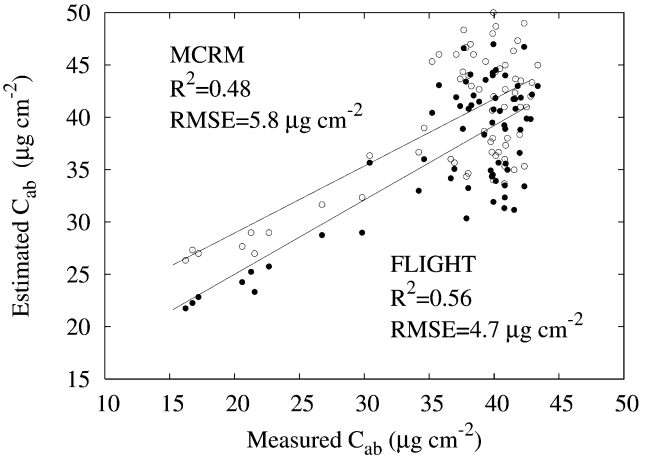

Figure 9. Scatterplot with measured vs. estimated chlorophyll values using multi-angular information and model inversion. Solid dots are used for 3D FLIGHT model.

obtained from the AHS sensor by flying four tracks over the orchard with different viewing conditions.

A simple linear regression was found to be largely dependent on viewing conditions. The main focus of this paper, however, was the effect of viewing conditions on the inversion of two state-of-the-art canopy models, coupled with the PROSPECT leaf radiative transfer model. A turbid medium model, MCRM, was tested first. Then, a more realistic model, FLIGHT, was tested. This 3D geometric-optical model is based on ray tracing and does account for influences of canopy architecture on reflectance. Both canopy models were successful in estimating chlorophyll concentration for optimal flight conditions, when data were measured perpendicular to the solar plane. A RMSE value just above $5\,\mu g\,cm^{-2}$ was obtained for both MCRM and FLIGHT. This result shows that chlorosis stress can be detected from canopy level through model inversion. However, the turbid medium model showed considerable differences between the results obtained for each individual track. Conversely, the 3D model was shown to be very robust to viewing geometry, with a persistent low RMSE value for each track (values between $5.4\,\mu g\,cm^{-2}$ and $6.9\,\mu g\,cm^{-2}$). A larger range of zenith angles would allow us to better estimate the full implication of the sensitivity to observation angles. Some indication is provided, but is based on synthetic data. A new flight campaign covering this aspect is recommended and is the subject of future research.

Finally, two methodologies were tested to combine multi-angular data for chlorophyll retrieval. For MCRM, the RMSE comes close to the single best observation (5.2–$5.8\,\mu g\,cm^{-2}$), while the value for R^2 improved from 0.44 to 0.48. Best results are obtained for the 3D model. The two methodologies improved both RMSE and R^2, with a minimum RMSE of $4.7\,\mu g\,cm^{-2}$ and a maximum R^2 value of $0.56\,\mu g\,cm^{-2}$.

The inversion of coupled canopy-leaf reflectance models for chlorophyll retrieval is a promising technique. However, special care must be taken when selecting the canopy model. For open canopies, turbid medium models are not robust to suboptimal viewing conditions. Though such conditions are often encountered in

operational conditions with large swath low resolution or pointable high resolution sensors. There are a lot of problems to resolve before precision agriculture becomes truly operational. However, recent improvement of canopy models accounting for canopy architecture, combined with cheaply available computing resources, are steps in the right direction.

Acknowledgments

We would like to thank the Belgian Science Policy Office (project SR/00/70) and the Spanish Ministry of Education MEC (project AGL2005-04049) for financing this work. We also acknowledge Dr. A. Kuusk, and Dr. M. Disney for providing their code for the MCRM model and Dr. L. Ingber for providing the ASA code.

References

ABUELGASIM, A.A., GOPAL, S. and STRAHLER, A.H., 1998, Forward and inverse modeling of canopy directional reflectance using a neural network. *International Journal of Remote Sensing*, **19**, pp. 453–471.

ALTON, P., NORTH, P., KADUK, J. and LOS, S., 2005, Radiative transfer modelling of direct and diffuse sunlight in a siberian pine forest. *Journal of Geophysical Research*, **110**, D23209.

BARNSLEY, M.J., SETTLE, J.J., CUTTER, M., LOBB, D. and TESTON, F., 2004, The PROBA/CHRIS mission: a low-cost smallsat for hyperspectral, multi-angle, observations of the earth surface and atmosphere. *IEEE Transactions on Geoscience and Remote Sensing*, **42**, pp. 1512–1520.

BARTON, C. and NORTH, P., 2001, Remote sensing of canopy light use efficiency using the photochemical reflectance index: model and sensitivity analysis. *Remote Sensing of Environment*, **78**, pp. 164–273.

BIESEMANS, J. and EVERAERTS, J., 2006, Image processing workflow for the PEGASUS HALE UAV payload. 2nd International Workshop "The Future of Remote Sensing." (ISPRS Inter-Commission Working Group I/V Autonomous Navigation). Available online at: http://www.pegasus4europe.com/pegasus/workshop/proceedings/htm (accessed 11 June 2008).

BLACKMER, T.M., SCHEPERS, J., VARVEL, G.E. and WALTER-SHEA, E., 1996, Nitrogen deficiency detection using reflected shortwave radiation from irrigated corn canopies. *Agronomy Journal*, **88**, pp. 1–5.

CAMPS-VALLS, G., BRUZZONE, L., ROJO-ROJO, J.L. and MELGANI, F., 2006, Robust support vector regression for biophysical variable estimation from remotely sensed images. *IEEE Geoscience and Remote Sensing Letters*, **3**, pp. 339–343.

CARTER, G.A., 1994, Ratios of leaf reflectances in narrow wavebands as indicators of plant stress. *International Journal of Remote Sensing*, **15**, pp. 697–703.

CHAPPELLE, E.W., KIM, M. and MCMURTREY, J., 1992, Ratio analysis of reflectance spectra (rars): An algorithm for the remote estimation of the concentrations of chlorophyll a, chlorophyll b, and carotenoids in soybean leaves. *Remote Sensing of Environment*, **39**, pp. 239–247.

CURRAN, P.J., 1989, Remote sensing of foliar chemistry. *Remote Sensing of Environment*, **30**, pp. 271–278.

CURRAN, P.J., DUNGAN, J.L., MACLER, B.A., PLUMMER, S.E. and PETERSON, D.L., 1992, Reflectance spectroscopy of fresh whole leaves for the estimation of chemical concentration. *Remote Sensing of Environment*, **39**, pp. 153–166.

DAUGHTRY, C.S.T., WALTHALL, C.L., KIM, M.S., DE COLSTOUN E.B. and MCMURTREY, J.E., 2000, Estimating corn leaf chlorophyll status from leaf and canopy reflectance. *Remote Sensing of Environment*, **74**, pp. 229–239.

DAWSON, T.P., NORTH, P., PLUMMER, S.E. and CURRAN, P.J., 2003, Forest ecosystem chlorophyll content: implications for remotely sensed estimates of net primary productivity. *International Journal of Remote Sensing*, **24**, pp. 611–617.

DINER, D.J., BECKERT, J., REILLY, T., BRUEGGE, C., CONEL, J., KAHN, R., MARTONCHIK, J., ACKERMAN, T., DAVIES, R., GERSTL, S., GORDON, H., MULLER, J.-P., MYNENI, R., SELLERS, R., PINTY, B. and VERSTRAETE, M.M., 1998, Multiangle imaging spectroradiometer (MISR) description and experiment overview. *IEEE Transactions on Geoscience and Remote Sensing*, **39**, pp. 1072–1087.

GAMON, J.A., 1992, A narrow-waveband spectral index that tracks diurnal changes in photosynthetic efficiency. *Remote Sensing of Environment*, **41**, pp. 35–44.

GITELSON, A.A. and MERZLYAK, M.N., 1996, Signature analysis of leaf reflectance spectra: Algorithm development for remote sensing of chlorophyll. *Journal of Plant Physiology*, **148**, pp. 494–500.

GROSSMAN, Y.L., USTIN, S.L., JACQUEMOUD, S., SANDERSON, E.W., SCHMUCK, G. and VERDEBOUT, J., 1996, Critique of stepwise multiple linear regression for the extraction of leaf biochemistry information from leaf reflectance data. *Remote Sensing of Environment*, **56**, pp. 1–12.

HABOUDANE, D., MILLER, J.R., TREMBLAY, N., ZARCO-TEJADA, P.J. and DEXTRAZE, L., 2002, Integration of hyperspectral vegetation indices for prediction of crop chlorophyll content for application to precision agriculture. *Remote Sensing of Environment*, **81**, pp. 416–426.

INGBER, L., Adaptive simulated annealing (asa). Lester Ingber Papers 93asa, Lester Ingber. Available at http://ideas.repec.org/p/lei/ingber/93asa.html.

JACQUEMOUD, S., BACOUR, C., POILVE, H. and FRANGI, J.P., 2000, Comparison of four radiative transfer models to simulate plant canopies reflectance-direct and inverse mode. *Remote Sensing of Environment*, **74**, pp. 471–481.

JACQUEMOUD, S., USTIN, S.L., VERDEBOUT, J., SCHMUCK, G., ANDREOLI, G. and HOSGOOD, B., 1996, Estimating leaf biochemistry using the PROSPECT leaf optical properties model. *Remote Sensing of Environment*, **56**, pp. 194–202.

KIM, M.S., DAUGHTRY, C., CHAPPELLE, E.W., Mcmurtrey III, J.E. and WALTHALL, C.L., 1994, The use of high spectral resolution bands for estimating absorbed photosynthetically active radiation. In *Proceedings of the 6th Symposium On Physical Measures and Signatures in Remote Sensing*, January, 1994, Val D'Isere, France, pp. 299–306.

KIMES, D., NELSON, R., MANRY, M. and FUNG, A., 1998, Attributes of neurall networks for extracting continuous vegetation variables from optical and radar measurements. *International Journal of Remote Sensing*, **19**, pp. 2639–2663.

KNYAZIKHIN, Y., MARTONCHIK, J., MYNENI, R., DINER, D. and RUNNING, S., 1998, Synergistic algorithm for estimating vegetation canopy leaf area index and fraction of absorbed photosynthetically active radiation from MODIS and MISR data. *Journal of Geophysical Research*, **103**(D24), pp. 32257–32276.

KOKALY, R.F. and CLARK, R.N., 1999, Spectroscopic determination of leaf biochemistry using band-depth analysis of absorption features and stepwise linear regression. *Remote Sensing of Environment*, **67**, pp. 267–287.

KUUSK, A., 1994, A multispectral canopy reflectance model. *Remote Sensing of Environment*, **50**, pp. 75–82.

KUUSK, A., 1995, Markov chain model of canopy reflectance. *Agricultural Forest Meteorology*, **76**, pp. 221–236.

KUUSK, A., 1998, Monitoring of vegetation parameters on large areas by the inversion of a canopy reflectance model. *International Journal of Remote Sensing*, **19**, pp. 2893–2905.

LACHENBRUCH, P., 1967, An almost unbiased method of obtaining confidence intervals for the probability of misclassification in discriminant analysis. *Biometrics*, **23**, pp. 639–645.

LICHTENTHALER, H.K., GITELSON, A.A. and LANG, M., 1996, Non-destructive determination of chlorophyll content of leaves of a green and an aurea mutant of tabacco by reflectance measurements. *Journal of Plant Physiology*, **148**, pp. 483–493.

MARTIN, M.E. and ABER, J.D., 1997, High spectral resolution remote sensing of forest canopy lignin, nitrogen and ecosystem process. *Ecological Applications*, **7**, pp. 431–443.

MILLER, J.R., HARE, E.W. and WU, J., 1990, Quantitative characterization of the vegetation red edge reflectance: An inverted-gaussian model. *International Journal of Remote Sensing*, **11**, pp. 1755–1773.

MYNENI, R., HALL, F., SELLERS, P. and MARSHAK, A., 1995, The interpretation of spectral vegetation indices. *IEEE Transactions on Geoscience and Remote Sensing*, **33**, pp. 481–486.

NORTH, P., 1996, Three-dimensional forest light interaction model using a Monte Carlo method. *IEEE Transactions on Geoscience and Remote Sensing*, **34**, pp. 946–956.

NORTH, P., 2002, Estimation of fAPAR, LAI and vegetation fractional cover from ATSR-2 imagery. *Remote Sensing of Environment*, **80**, pp. 114–121.

PEÑUELAS, J., FILELLA, I. and GAMON, J.A., 1995a, Assessment of photsynthetic radiation-use efficiency with spectral reflectance. *New Phytologist*, **131**, pp. 291–296.

PEÑUELAS, J., GAMON, J.A., FREDEEN, A.L., MERINO, J. and FIELD, C.B., 1994, Reflectance indices associated with physiological changes in nitogen- and water-limited sunflower leaves. *Remote Sensing of Environment*, **48**, pp. 135–146.

PEÑUELAS, J., FILELLA, I. and GAMON, J.A., 1995b, Assessment of photosynthetic radiation-use efficiency with spectral reflectance at the leaf and canopy levels. In *Proceedings of the International Colloguium, Photosynthesis and Remote Sensing*, G. Guyot (Ed), August 1995, Montpellier, France, pp. 129–134.

PINTY, B., WIDLOWSKI, J.L., TABERNER, M., VERSRTAETE, M.M., DISNEY, M., GASCON, F., GASTELLU, J.P., JIANG, L., KUUSK, A., LEWIS, P., LI, X., NILSON, W.N.-M.T., NORTH, P., QIN, W., SU, L., TANG, S., THOMPSON, R., WANG, W.V.H., WANG, J., YAN, G. and ZANG, H., 2004, Radiation transfer model intercomparison (RAMI) exercise: results from the second phase. *Journal of Geophysical Research*, **109**, D06210.

PRAGNÈRE, A., BARET, F., WEISS, M., MYNENI, R.B., KNYAZIKHIN, Y. and WANG, L.B., 1999, Comparison of three radiative transfer model inversion techniques to estimate canopy biophysical variables from remote sensing data. In *Proceedings of the International Geoscience and Remote Sensing Symposium* (IGARSS'99), Hamburg, Germany.

RICHTER, R., 2004, Atmospheric/topographic correction for airborne imagery. ATCOR-4 user guide version 3.1. Technical report, DLR, Wessling, Germany.

ROUSE, J.W., HAAS, R.H., SCHELL, J.A. and DEERING, D.W., 1973, Monitoring vegetation systems in the great plains with ERTS. In *Third ERTS Symposium*, Vol. NASA SP-351 I, pp. 309–317.

SCHLERF, M. and ATZBERGER, C., 2006, Inversion of a forest reflectance model to estimate structural canopy variables from hyperspectral remote sensing data. *Remote Sensing of Environment*, **100**, pp. 281–294.

SMITH, J.A., 1993, Lai inversion using back propagation nerual network trained with multiple scattering model. *IEEE Transactions on Geoscience and Remote Sensing*, **31**, pp. 1102–1106.

VERHOEF, W., 1984, Light scattering by leaf layers with application to canopy reflectance modeling: The SAIL model. *Remote Sensing of Environment*, **16**, pp. 125–141.

VERSTRAETE, M., PINTY, B. and MYNENI, R., 1996, Potential and limitations of inormation extraction on the terrestrial biosphere from satellite remote-sensing. *Remote Sensing of Environment*, **58**, pp. 201–214.

VILLALOBOS, F.J., ORGAZ, F. and MATEOS, L., 1995, Non-destructive measurement of leaf area in olive (olea europaea l.) trees using a gap inversion method. *Agricultural and Forest Meteorology*, **73**, pp. 29–42.

WEISS, M., BARET, F., MYNENI, R.B., PRAGNÈRE, A. and KNYAZIKHIN, Y., 2000, Investigation of a model inversion technique to estimate canopy biophysical variables from spectral and directional reflectance data. *Agronomie*, **20**, pp. 3–22.

WESSMAN, C.A., ABER, J.D., PETERSON, D.L. and MELILLO, J.M., 1988, Remote sensing of canopy chemistry and nitrogen cycling in temperate forest ecosystems. *Nature*, **335**, pp. 154–156.

ZARCO-TEJADA, P.J., MILLER, J.R., MOHAMMED, G.H., NOLAND, T.L. and SAMPSON, P.H., 2001, Scaling-up and model inversion methods with narrow-band optical indices for chlorophyll content estimation in closed forest canopies with hyperspectral data. *IEEE Transactions on Geoscience and Remote Sensing*, **39**, pp. 1491–1507.

ZARCO-TEJADA, P.J., MILLER, J.R., MORALES, A., BERJÓN, A. and AGÜERA, J., 2004, Hyperspectral indices and model simulation for chlorophyll estimation in open-canopy tree crops. *Remote Sensing of Environment*, **90**, pp. 463–476.